# Supporting Information

## Ripaud et al. 10.1073/pnas.1421313111

### SI Materials and Methods

**Plasmids.** pYES2L-25Q-GFP and pYES2L-103Q-GFP were generated by replacing the *URA3* selection marker from pYES2-25Q-GFP and pYES2-103Q-GFP [kind gifts from M. Y. Sherman (Boston University School of Medicine, Boston)] (1) with *LEU2* using the pUL9 marker swap plasmid (2). The plasmid encoding Rnq1-GFP was a kind gift from S. Lindquist (Massachusetts Institute of Technology, Cambridge, MA) (3). Potential suppressors were cloned with or without N-terminal myc-tags into pCM190 (4). Full-length and truncated forms of *GTS1*, *NAB3*, *SIS1*, *SOK1*, *SUC2*, *TAF12*, and *YCK1* were inserted into the multiple cloning site of pCM190 via the NotI and PstI restriction sites, whereas the N terminus of *SUP35* was inserted into pCM190 via BamHI and NotI. Full-length and truncated *MCM1* was inserted into pRS426 (5) via XhoI and HindIII.

***Antibodies.*** Anti-mouse IgG (peroxidase conjugated) and anti-mouse IgG (Cy-3 conjugated) were purchased from Sigma, anti-GFP was from Roche, and anti-myc was from Santa Cruz.

***Western Blot Analysis and Filter Retardation Assay.*** SDS/PAGE and Western blot analysis were performed according to standard procedures. For the filter retardation assay (6, 7), protein samples (25 μg) were heated at 95 °C for 10 min in 2% (wt/vol) SDS and 50 mM DTT and filtered through a 0.2-μm cellulose acetate membrane (Whatman) using a Hoefer PR 648 slot-blot manifold. Captured aggregates were detected by incubation for 1 h with anti-GFP antibody followed by 1 h with peroxidase-coupled anti-mouse-IgG and chemiluminescence detection using a LAS-3000 Image Reader (Fujifilm) and AIDA image analysis software (version 4.15; Raytest).

**Immunoprecipitation.** Samples containing 1 mg of protein were incubated with 10 μL of anti-GFP antibody or with 15 μL anti-myc antibody for 1 h at 4 °C with slow agitation; 80 μL Protein A-Sepharose (Sigma) was added, and the samples were further incubated at 4 °C for 2 h with agitation. After two washing steps with lysis buffer, proteins were eluted using hot SDS-loading buffer, followed by SDS/PAGE and Western blotting.

**Yeast Methods.**

***Yeast strains used in this study.*** The yeast strains used in this study are the YPH499 (MATa [RNQ$^+$] ura3-52 lys2-801_amber ade2-101_ochre trp1Δ63 his3Δ200 leu2Δ1) and YPH 500 (MATα [RNQ$^+$] ura3-52 lys2-801_amber ade2-101_ochre trp1Δ63 his3Δ200 leu2Δ1) (8) or the BY4741 strain (MATa [RNQ$^+$] his3Δ1 leu2Δ0 met15Δ0 ura3Δ0) (Open Biosystems).

YPH499 [*rnq*$^-$] was obtained by growing the cells 72 h in yeast extract peptone dextrose (YPD) + 5 mM GdmCl (9, 10). One clone was selected that had lost the aggregation of Rnq1p using a Rnq-GFP fusion as read-out.

***Yeast media.*** Yeast media were prepared as previously described (11). WT yeast were grown in standard synthetic complete (SC) [0.67% yeast nitrogen base and 2% (wt/vol) glucose] or YPD medium [20 g/L Difco peptone, 10 g/L yeast extract, and 2% (wt/vol) glucose], and transformants were grown in synthetic media lacking the indicated amino acids.

***Growth assays.*** Yeast transformants were grown overnight in selective media with 2% (wt/vol) glucose as the sole carbon source. Cultures were adjusted to equal concentrations based on $OD_{600}$. Cells were spotted in serial 10-fold dilutions. Equal spotting was controlled by spotting on plates with glucose as a carbon source in parallel with galactose plates. Plates were air-dried and incubated 3–5 d at 30 °C. Images were acquired using a LAS-3000 Image Reader (Fujifilm).

***Induction.*** *GAL1* promotor-controlled proteins were induced by switching to growth in selective media containing 2% (wt/vol) galactose after growing yeast cells to midlog phase at 30 °C in selective media containing glucose as the sole carbon source.

*CUP1* promotor-controlled protein expression was induced by growth in media containing 50 mM $Cu_2SO_4$. Expression of proteins under the control of a tetracycline-repressible promotor was induced by switching from a selective media containing doxycycline to a media without doxycycline.

***Transformation.*** Transformation of yeast was performed by the lithium acetate method as described previously (12). In brief, yeast and plasmid DNA was resuspended in polyethylene glycol (PEG)/lithium acetate (LiAc) solution [40% (wt/vol) PEG and 0.1 M LiAc in Tris-EDTA buffer] and incubated for 1 h at 30 °C. After this, 70 μL DMSO was added, and the cells were incubated for 20 min at 42 °C. Cells were then plated on the appropriate selection media.

***Cell lysis.*** Yeast cells were lysed using glass beads; 50 $OD_{600}$ of cells were harvested and washed twice in ice-cold sterile $H_2O$, before resuspension in ice-cold lysis buffer [25 mM Tris/HCl pH 7.5, 50 mM KCl, 10 mM $MgCl_2$, 1 mM EDTA, 5% (vol/vol) glycerol, 1 mM DTT, 1 mM PMSF, and 1× protease inhibitor mixture; Roche]. Next, acid-washed glass beads were added to the sample, and cells were disrupted in a FastPrep-24 homogenizer (MP Biomedicals). The lysate was separated from the beads and precleared by centrifugation for 5 min at 2,000 × *g*. The supernatant was transferred to a new tube and treated for 1 h at 4 °C with benzonase (50 U) (Merck).

***Identification and retesting of suppressors.*** Elimination of false positives was done as follows. Drop tests were performed as described above to confirm that the suppression of toxicity was reproducible. Expression of 103Q-GFP was verified by fluorescence microscopy after growth on SC selection medium. Clones without any GFP signal, due to loss or recombination of the pYES2L-103Q-GFP plasmid, were discarded. Finally, the remaining clones were mated with YPH500 [*RNQ*$^+$] and the toxicity of 103Q-GFP in the resulting diploids was tested by a drop test. False positives due to loss of [*RNQ*$^+$] showed no suppression of toxicity in the diploids and were discarded.

The remaining 40 clones were grown on glucose SC selection medium without Ura and with Leu. Clones that lost the pYES2L-Htt-GFP plasmid were selected on the basis of their inability to grow on SC selection medium without Leu. Plasmids were extracted from these clones using a miniprep kit (Qiagen) according to the manufacturer's instructions with the following modifications: 10 $OD_{600}$ of yeast cells was resuspended in P1 and P2 buffers, and then glass beads and 250 μL phenol:chloroform: isoamylalcohol (25:24:1) were added. Cells were disrupted by vortexing 2 × 1 min. After centrifugation, the supernatant was mixed with Qiagen N3 buffer and then further processed according to the manufacturer's instructions. The purified plasmids were transformed into *Escherichia coli* by electroporation.

Minipreps were performed from four independent *E. coli* colonies for each clone from the screen and analyzed by restriction analysis to determine whether clones had been transformed by more than one YEp13 plasmid. Each individual YEp13 plasmid identified was then transformed in YPH499 + pYES2L-103Q-GFP as described above. Drop tests were performed on selective SC plates as described above, and clones able to suppress toxicity were selected.

Positive plasmids were then sequenced. For inserts that contained more than one gene, each gene was individually cloned into pCM190 or pRS426 and retested.

**Fluorescence Microscopy.** Fluorescence imaging was carried out on a Zeiss Axiovert 200M fluorescence microscope with a 100× oil lens (NA 1.3; Zeiss). Digital images were acquired with a Zeiss Axiocam HRM camera und processed using the ImageJ software (imagej.nih.gov/ij/). Images were resized, and brightness and contrast were adjusted in ImageJ and Adobe Photoshop CS5. Figures were prepared in Adobe Illustrator CS5.

## Molecular Modeling.

***Simulation setup.*** We performed two distinct sets of simulations with 2 + 1 molecules. The stoichiometry of QAR:35Q molecules was 2:1 in one set and 1:2 in the other set. All simulations were performed using the CAMPARI simulation package (campari.sourceforge.net) using the ABSINTH implicit solvation model and force field paradigm and partial charges based on the OPLS-AA/L molecular mechanics force field as implemented in the abs3.2_opls.prm parameter file (13, 14). The molecules were enclosed in spherical droplets of a radius of 200 Å. This choice guards against unrealistic associations that result from the effects of confinement, which can happen in simulation droplets of smaller size. All polypeptides were modeled in atomic detail. The sequences for 35Q molecules are of the form Ac-$Q_{35}$-Nme and for QAR they are Ac-$(QA)_6$-QV-$(QA)_7$-Nme. Here, Ac and Nme refer to the capping groups *N*-acetyl and *N′*-methylamide, respectively. These capping groups ensure that the polypeptides are not in their zwitterionic form and that the intermolecular associations that we observe are not influenced by strong and spurious electrostatic interactions between charged N and C termini.

***Thermal replica exchange.*** We use thermal replica exchange in combination (15, 16) with Markov Chain Metropolis Monte Carlo (MCC) (14) moves to enhance conformational sampling. In replica exchange simulations, one creates copies of the simulation system and assigns different simulation temperatures to each replica. At higher temperature, the system can negotiate energy barriers more easily than at lower simulation temperatures. The simulations corresponding to each temperature are run independently, and at randomly chosen intervals, a swap of conformations is proposed between pairs of replicas, each corresponding to a different temperature. The proposed swap is accepted or rejected in accordance with the prescription to microscopic reversibility.

In our simulation approach, each independent replica exchange simulation contained 14 different replicates that follow the temperature schedule: $T$ = 288, 298, 305, 315, 325, 335, 340, 345, 350, 355, 360, 365, 375, and 385 K. For each thermal replica exchange simulation, we used $10^7$ independent equilibration steps. Statistics for analysis were obtained from the production runs, which were based on $5.15 \times 10^7$ Monte Carlo steps. Conformational swaps between neighboring replicas were attempted every 50,000 steps. Three independent replica exchange simulations were conducted for each system, and the results were stitched together using the temperature-dependent weighted histogram analysis method (17). This method allows us to obtain statistically robust assessments of the conformational distributions of individual molecules and molecular clusters.

***MMC move sets.*** In each set of MMC simulations enhanced by thermal replica exchange, the molecules are fully flexible, and the degrees of freedom include the backbone bond torsion angles φ, ψ, and ω, the side-chain torsion angles χ, and the rigid body coordinates of all three polypeptides. The move sets allow for a combination of local and global conformational changes of the polypeptide degrees of freedom. Local changes correspond to finite perturbations with a defined maximum step size. Global changes correspond to a full randomization of a particular degree of freedom. The combination of these changes allows different length scales to be probed. Details of the move sets used for each of the simulations including the frequency of each move type and maximum step sizes for finite perturbations are summarized in Table S1.

***Clustering.*** Observables were collected every 5,000 steps at 315 K. These frames were filtered such that every 10th frame was collected from each simulation. The frames were further filtered to include only those frames in which molecules had at least one contact between glutamine or alanine/valine residues such that all molecules in the simulations were associated. A contact was defined as two atoms from different residues being within 3.5 Å of each other. The conformation of each remaining frame was represented as a $1 \times n_d$ vector $\mathbf{V}_c$, where $n_d = \frac{N(N+1)}{2}$, $N$ is the number of residues, and $\mathbf{V}_c = \{d_{11}, d_{12}, \ldots, d_{1N}, d_{22}, \ldots, d_{N,N}\}$. Each $d_{ij}$ corresponds to the spatial distance between residues $i$ and $j$. Here, $d_{ij} = \frac{1}{Z_{ij}} \cdot \sum_{m \in i} \sum_{n \in j} |\mathbf{r}_m^i - \mathbf{r}_n^j|$, where $Z_{ij}$ is the number of unique pairwise interatomic distances between residues $i$ and $j$, and $\mathrm{r}_m^i$ and $\mathrm{r}_n^j$ are the position vectors of atom $m$ within residue $i$ and atom $n$ within residue $j$, respectively. The pairwise dissimilarity measure $\mathcal{D}_{kl} = 1 - \cos(\Omega_{kl})$, where $\cos(\Omega_{kl}) = \frac{\mathbf{V}_k \cdot \mathbf{V}_l}{|\mathbf{V}_k||\mathbf{V}_l|}$, was used to compare conformations $k$ and $l$ given by vectors $\mathbf{V}_k$ and $\mathbf{V}_l$, respectively (18). An agglomerative hierarchical cluster tree was then determined using MATLAB's linkage function (www.mathworks.com) using the average distance between clusters. Final clusters were generated using MATLAB's cluster function, which prunes branches off the previously generated agglomerative hierarchical cluster tree. Then, the conformation, $C$, with the minimum dissimilarity from all other conformations within a cluster is depicted. Specifically, $C = k$, where $k$ is the conformation that corresponds to $\min(\sum_l \mathcal{D}_{kl})$.

***Calculation of cumulative distribution functions of distances between centers of mass for pairs of molecules.*** To generate CDFs, the distance between the centers of mass of molecules in the three molecule simulations was determined at every 5,000 steps. This sampling resulted in $N$ frames for each simulation, where $n$ = 10,300. To generate error bars, 100 bootstrap trials were performed with a sample size of 0.1 N. T-WHAM (17) was used to reweight the simulation results to the original set of simulation temperatures. The cumulative distribution functions plotted quantify the distance between the centers of mass for both homo- and heterotypic pairings for the reweighted simulation data at the target temperature of 315 K.

## Interactome Analysis.

***Immunoprecipitation.*** Yeasts were grown as preculture in selective medium, expressing suppressor proteins where indicated, until the stationary phase was reached. Overnight cultures were grown in SC galactose medium to additionally express 103Q-GFP until late exponential phase ($OD_{600} \sim 0.8$) was reached. Yeast lysates were prepared in lysis buffer [25 mM Tris/HCl, pH 7.5, 50 mM KCl, 10 mM $MgCl_2$, 5% (vol/vol) glycerol, 1% Nonidet P-40, 1 mM DTT, 1 mM PMSF, complete protease inhibitors (Roche), and PhosSTOP phosphatase inhibitors (Roche)] using a FastPrep-24 homogenizer with CoolPrep adaptor (MP Biomedical). Total lysates were centrifuged at 500 × *g* for 10 min at 4 °C to remove unbroken cells and treated with benzonase over night at 4 °C. Three milligrams of protein was diluted to 800 μL, and 8 μL was set aside as input control. The remaining solution was incubated with 50 μL anti-GFP μMACS MicroBeads (Miltenyi Biotech) for 1 h at 4 °C and afterward loaded on μMACS columns (Miltenyi Biotech). After four washes with wash buffer I [50 mM Tris/HCl, pH 7.5, 150 mM NaCl, 5% (vol/vol) glycerol, and 0.05% Nonidet P-40] and two additional washing steps with wash buffer II [50 mM Tris/HCl, pH 7.5, 150 mM NaCl, and 5% (vol/vol) glycerol], proteins were digested on the beads using elution buffer I (50 mM Tris/HCl, pH 7.5, 8 M urea, 1 mM DTT, and 150 ng LysC) for 1 h and elution buffer

II (50 mM Tris/HCl, pH 7.5, 5 mM chloroacetamide, and 150 ng trypsin) for an additional hour. After elution, additional trypsin (500 ng) and thiourea (final concentration 100 mM) were added for a further 16 h of digestion.

***Sample preparation for MS.*** Before the peptide mix was subjected to LC-MS, salts were removed via C18 StageTips (19).

***LC-MS/MS.*** LC (Thermo Scientific EASY-nLC 1000 HPLC) with in-house packed columns (75-μm inner diameter, 20-cm length, 1.9-μm C18 particles; Dr. Maisch GmbH) was used to separate peptides at 50 °C in an 85-min gradient from 98% (vol/vol) buffer A (0.5% formic acid) and 2% (vol/vol) buffer B [0.5% formic acid, 80% (vol/vol) acetonitrile] to 60% (vol/vol) buffer B at 250 nL/min. An Orbitrap mass spectrometer (Q Exactive; Thermo Fisher Scientific) (20) was directly coupled to the LC via a nano electrospray source. The Q Exactive was operated in a data-dependent mode.

The survey scan range was set to 300–1,650 $m/z$, with a resolution of 70,000. Up to the 10 most abundant isotope patterns with a charge ≥2 were subjected to higher-energy collisional dissociation (21) fragmentation at a normalized collision energy of 25, an isolation window of 3 Th, and a resolution of 17,500 at $m/z$ 200. Data were acquired using the Xcalibur software (Thermo Scientific).

***Data analysis and statistics.*** We used the MaxQuant software (v 1.4.3.19) (22) and Andromeda search engine (23) to process MS raw data searching against the UniProtKB Yeast FASTA database (6/2012) using standard settings (24). Data were filtered for common contaminants ($n$ = 247), reverse identification, and proteins only identified with modifications. The minimum required peptide length for identification was set to seven amino acids. Quantification was performed using the MaxLFQ label-free algorithms (25). For bioinformatic analysis and visualization, we used PERSEUS, which is part of MaxQuant and the R framework (26). Missing values were imputed with a normal distribution (width = 0.3; shift = 1.8). Significantly enriched proteins in pairwise interactome comparisons were determined by $t$ test statistics [permutation-based false discovery rate (FDR) of 5% and S0 of 1] (27). For 1D annotation enrichment on the Welch test difference, we applied a Benjamini–Hochberg-corrected FDR cutoff of 2% (28).


1. Meriin AB, et al. (2002) Huntington toxicity in yeast model depends on polyglutamine aggregation mediated by a prion-like protein Rnq1. *J Cell Biol* 157(6):997–1004.
2. Cross FR (1997) 'Marker swap' plasmids: Convenient tools for budding yeast molecular genetics. *Yeast* 13(7):647–653.
3. Sondheimer N, Lindquist S (2000) Rnq1: An epigenetic modifier of protein function in yeast. *Mol Cell* 5(1):163–172.
4. Garí E, Piedrafita L, Aldea M, Herrero E (1997) A set of vectors with a tetracycline-regulatable promoter system for modulated gene expression in Saccharomyces cerevisiae. *Yeast* 13(9):837–848.
5. Christianson TW, Sikorski RS, Dante M, Shero JH, Hieter P (1992) Multifunctional yeast high-copy-number shuttle vectors. *Gene* 110(1):119–122.
6. Scherzinger E, et al. (1997) Huntingtin-encoded polyglutamine expansions form amyloid-like protein aggregates in vitro and in vivo. *Cell* 90(3):549–558.
7. Wanker EE, et al. (1999) Membrane filter assay for detection of amyloid-like polyglutamine-containing protein aggregates. *Methods Enzymol* 309:375–386.
8. Sikorski RS, Hieter P (1989) A system of shuttle vectors and yeast host strains designed for efficient manipulation of DNA in Saccharomyces cerevisiae. *Genetics* 122(1):19–27.
9. Tuite MF, Mundy CR, Cox BS (1981) Agents that cause a high frequency of genetic change from [psi+] to [psi-] in Saccharomyces cerevisiae. *Genetics* 98(4):691–711.
10. Eaglestone SS, Ruddock LW, Cox BS, Tuite MF (2000) Guanidine hydrochloride blocks a critical step in the propagation of the prion-like determinant [PSI(+)] of Saccharomyces cerevisiae. *Proc Natl Acad Sci USA* 97(1):240–244.
11. Guthrie C, Fink GR (1991) *Guide to Yeast Genetics and Molecular Biology* (Academic Press, San Diego).
12. Gietz RD, Schiestl RH, Willems AR, Woods RA (1995) Studies on the transformation of intact yeast cells by the LiAc/SS-DNA/PEG procedure. *Yeast* 11(4):355–360.
13. Vitalis A, Pappu RV (2009) ABSINTH: A new continuum solvation model for simulations of polypeptides in aqueous solutions. *J Comput Chem* 30(5):673–699.
14. Vitalis A, Pappu RV (2009) Methods for Monte Carlo simulations of biomacromolecules. *Annu Rep Comput Chem* 5:49–76.
15. Mitsutake A, Sugita Y, Okamoto Y (2001) Generalized-ensemble algorithms for molecular simulations of biopolymers. *Biopolymers* 60(2):96–123.
16. Mitsutake A, Sugita Y, Okamoto Y (2003) Replica-exchange multicanonical and multicanonical replica-exchange Monte Carlo simulations of peptides. II. Application to a more complex system. *J Chem Phys* 118(14):6676–6688.
17. Chodera JD, Swope WC, Pitera JW, Seok C, Dill KA (2007) Use of the weighted histogram analysis method for the analysis of simulated and parallel tempering simulations. *J Chem Theory Comput* 3(1):26–41.
18. Lyle N, Das RK, Pappu RV (2013) A quantitative measure for protein conformational heterogeneity. *J Chem Phys* 139(12):121907.
19. Rappsilber J, Mann M, Ishihama Y (2007) Protocol for micro-purification, enrichment, pre-fractionation and storage of peptides for proteomics using StageTips. *Nat Protoc* 2(8):1896–1906.
20. Michalski A, et al. (2011) Mass spectrometry-based proteomics using Q Exactive, a high-performance benchtop quadrupole Orbitrap mass spectrometer. *Mol Cell Proteomics* 10(9):M111 011015.
21. Olsen JV, et al. (2006) Global, in vivo, and site-specific phosphorylation dynamics in signaling networks. *Cell* 127(3):635–648.
22. Cox J, Mann M (2008) MaxQuant enables high peptide identification rates, individualized p.p.b.-range mass accuracies and proteome-wide protein quantification. *Nat Biotechnol* 26(12):1367–1372.
23. Cox J, et al. (2011) Andromeda: A peptide search engine integrated into the MaxQuant environment. *J Proteome Res* 10(4):1794–1805.
24. Meissner F, Scheltema RA, Mollenkopf HJ, Mann M (2013) Direct proteomic quantification of the secretome of activated immune cells. *Science* 340(6131):475–478.
25. Cox J, et al. (2014) Accurate proteome-wide label-free quantification by delayed normalization and maximal peptide ratio extraction, termed MaxLFQ. *Mol Cell Proteomics* 13(9):2513–2526.
26. R Core Team (2014) *R: A Language and Environment for Statistical Computing* (R Foundation for Statistical Computing, Vienna).
27. Tusher VG, Tibshirani R, Chu G (2001) Significance analysis of microarrays applied to the ionizing radiation response. *Proc Natl Acad Sci USA* 98(9):5116–5121.
28. Cox J, Mann M (2012) 1D and 2D annotation enrichment: A statistical method integrating quantitative proteomics with complementary high-throughput data. *BMC Bioinformatics* 13(Suppl 16):S12.

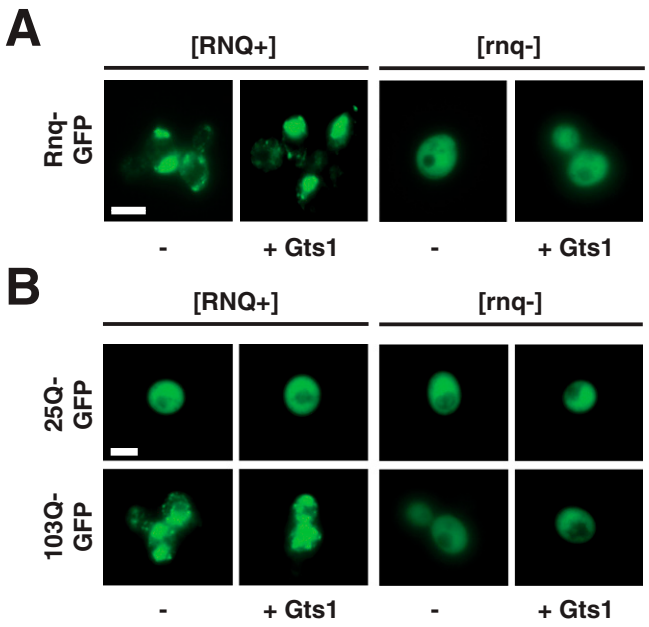


**Fig. S1.** Gts1p expression is not affecting Rnq1p prion status or 103Q-GFP inclusion formation. (*A*) Gts1p expression does not change the Rnq1p prion status. YPH499 [*RNQ*$^+$] and YPH499 [*rnq*$^-$] cells were transformed with plasmids encoding Rnq1-GFP and Gts1p. Gts1p expression was induced overnight in SC medium without doxycycline. Rnq1-GFP expression was induced by $Cu_2SO_4$ for 6–8 h before analysis of the cells by fluorescence microscopy. (*B*) 103Q-GFP inclusion formation is dependent on [*RNQ*$^+$] but independent of Gts1p expression. YPH499 [*RNQ*$^+$] and YPH499 [*rnq*$^-$] cells were transformed with plasmids encoding 25Q/103Q-GFP and Gts1p. Gts1p expression was induced over night by growth in SC medium without doxycycline. The cells were diluted in the morning in SC medium containing glucose or galactose and observed after 2–4 h by fluorescence microscopy. (Scale bar, 5 μm.)

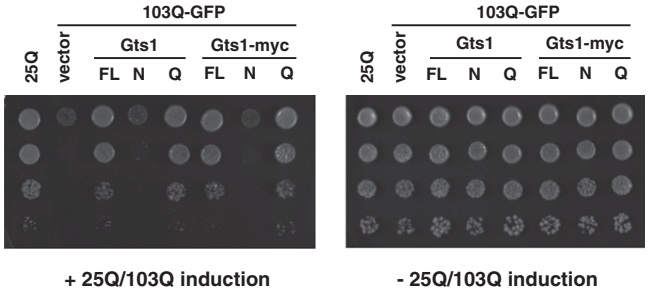


**Fig. S2.** Addition of a myc-tag does not affect the function of Gts1p as a suppressor of 103Q-GFP toxicity. *GTS1* WT and myc-tagged alleles were cloned under the control of the tetracycline repressible promoter in pCM190 and transformed in YPH499 + 25Q/103Q-GFP. Cells were grown in glucose medium without doxycycline to preinduce the suppressors. Then serial dilutions were spotted on galactose plates without doxycycline to coexpress 25Q/103Q-GFP and the suppressors (*Left*) or on glucose as control (*Right*). The galactose plates were incubated for 4–5 d at 30 °C and the glucose plates for 2–3 d.

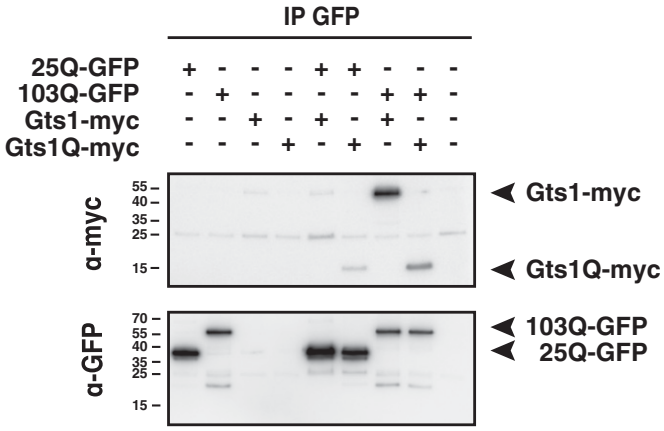


**Fig. S3.** 103Q-GFP physically interacts with Gts1-myc and Gts1Q-myc. YPH499 cells were transformed with 25Q/103Q-GFP and Gts1-myc/Gts1Q-myc. The different versions of Gts1p were preinduced before induction of 25Q/103Q-GFP. After cell lysis, anti-GFP coupled beads were used for immunoprecipitation (IP), followed by SDS/PAGE and Western blotting using anti-GFP and anti-myc antibodies.

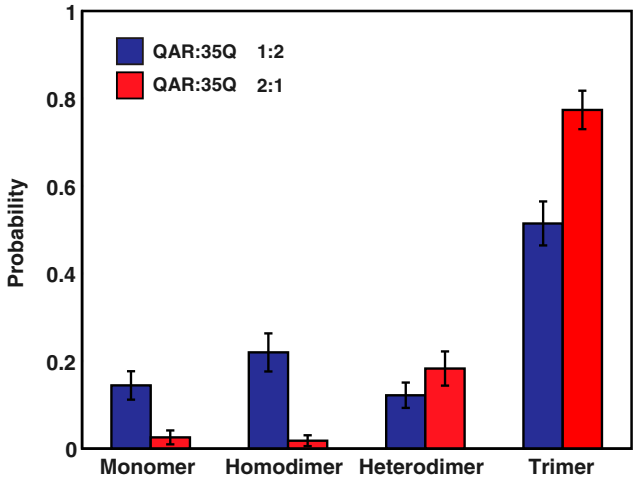


**Fig. S4.** Species distributions obtained from atomistic simulations with different stoichiometries for QAR:35Q molecules. The results are shown for 315 K. This figure quantifies the probabilities of realizing monomers, dimers (heterodimers and homodimers), and trimers in the equilibrium distribution obtained at 315 K.

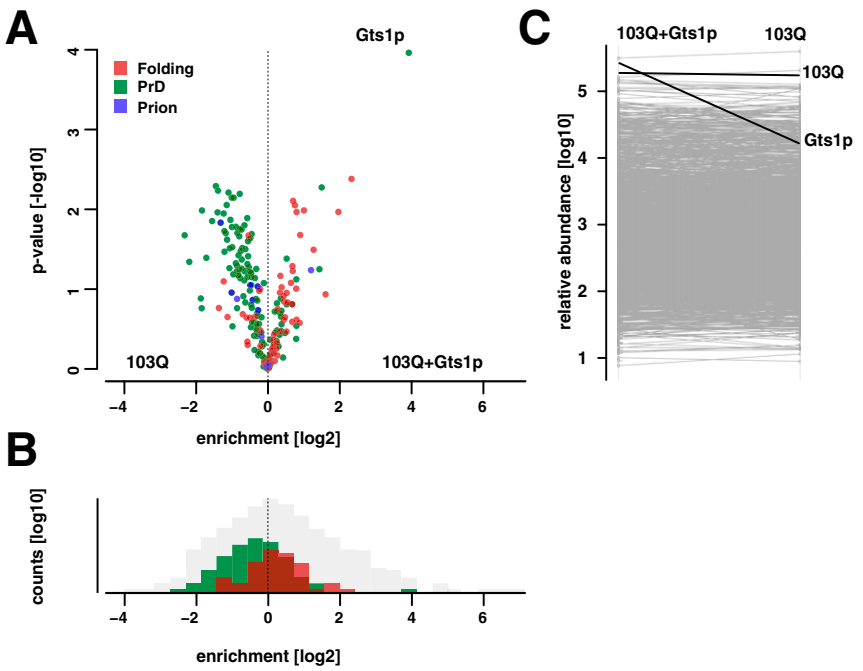


**Fig. S5.** Gts1p changes the 103Q-GFP interactome. (*A*) Analysis of 103Q-GFP interactors in presence or absence of Gts1p was performed as described in Fig. 5. Interactors involved in protein folding are labeled in red, interactors with a predicted prion domain (PrD) in green, and proteins annotated as prions in blue. The comparison of *P* value and difference of means from *t* test statistics shows which proteins are enriched, unchanged, or depleted in the comparison of the two interactomes. (*B*) Binned distribution of proteins in the pairwise comparison of interactomes shows converse shifts for proteins with a predicted PrD and those involved in protein folding. (*C*) Relative abundance of 103Q-GFP and Gts1p after immunoprecipitation of 103Q-GFP. MaxLFQ values were normalized by division with the molecular weight of the respective proteins to compare the abundance of different proteins within a proteome. Due to the lack of tryptic peptides within the N terminus of Htt, 103Q-GFP levels were approximated by GFP abundance.

**Table S1. Move set details for MMC the 2 + 1 molecule simulations**

| Move type | Frequencies, % | $f_\Delta$, % | Step size (maximum) |
|---|---|---|---|
| Rigid body | 30 | 50 | 10 Å, 20° |
| Side-chain, χ | 21 | 40 | 2,* 30° |
| Concerted rotation | 4.9 | — | — |
| ω | 4.41 | 90 | 5° |
| Backbone pivots φ, ψ | 39.69 | 70 | 10° |

The fraction of moves allocated to finite perturbations for each move type is denoted by $f_\Delta$. The remaining fraction of moves is assigned to full randomization for each move type. The fourth column gives the maximum step size for each degree of freedom. Rigid body moves include maximum step sizes for both translational and rotational moves, respectively.
*The maximum number of χ angles sampled within a single side-chain move.

**Dataset S1. MaxLFQ quantitative interactome data and identifiers**

Dataset S1

(*A*) MaxLFQ protein intensities (log2) for 103Q-GFP and Gts1p, 103Q-GFP and Gts1Q, and 25Q-GFP and 103Q-GFP immunoprecipitations. Uniprot protein IDs and protein and gene names are listed. (*B*) List of all identified proteins annotated as Prion, PrD, or with the GOBP term "protein folding." Imputed and filtered MaxLFQ intensities (reverse proteins, proteins only identified with modifications, and contaminants as well as proteins that are not annotated for either "prion" [Alberti et al. (1); Uniprot Keywords] or "protein folding" (GOBP) with *t* test statistics for Gts1Q vs. 103Q-GFP and Gts1p vs. 103Q-GFP. (*C*) List of all proteins significantly changed by Gts1Q expression. Differences and *P* values of protein intensities of all proteins significantly changed by Gts1Q expression are listed. Significant outliers were determined by Welch *t* test (S0: 1, FDR: 0.05).

1. Alberti S, Halfmann R, King O, Kapila A, Lindquist S (2009) A systematic survey identifies prions and illuminates sequence features of prionogenic proteins. *Cell* 137(1):146–158.